 doi:10.20944/preprints201608.0008.v1

Article

Computational Fluid Dynamics (CFD) Mesh Independency Study of A Straight Blade Horizontal Axis Tidal Turbine

Siddharth Suhas Kulkarni*, Craig Chapman, Hanifa Shah

Knowledge Based Engineering Lab, Birmingham City University, Millennium Point, Curzon Street, Birmingham, B4 7XG, UK; siddharth.kulkarni@bcu.ac.uk; craig.chapman@bcu.ac.uk; hanifa.shah@bcu.ac.uk
* Correspondence: siddharth.kulkarni@bcu.ac.uk; Tel.: +44-121-331-2420

Abstract: This paper numerically investigates a 3D mesh independency study of a straight blade horizontal axis tidal turbine modelled using Computational Fluid Dynamics (CFD). The solution was produced by employing two turbulence models, the standard k-ε model and Shear Stress Transport (SST) in ANSYS CFX. Three parameters were investigated: mesh resolution, turbulence model, and power coefficient in the initial CFD, analysis. It was found that the mesh resolution and the turbulence model affect the power coefficient results. The power coefficients obtained from the standard k-ε model are 15% to 20% lower than the accuracy of the SST model. It can also be demonstrated that the torque coefficient increases with the increasing Tip Speed Ratio (TSR), but drops drastically after TSR = 5 and k-ε model failing to capture the non-linearity in the torque coefficient with the increasing TSR.

Keywords: horizontal axis tidal turbine; Computational Fluid Dynamics; mesh independency; NACA 0018

PACS: J0101

1. Introduction

Tidal energy is a renewable electricity source based on the conversion of kinetic energy of moving water into mechanical power to drive generators [1]. It has fewer CO_2 emissions, and it has minimal reliance on fossil fuels. It is one of the many sources to address concerns over climate change [2]. As there is a need to identify and use more sustainable sources of power generation tidal energy will gain more attention. Tides result from the gravitational pull of the moon. "As 71% of the earth's surface is covered by water, energy can be harnessed on a large scale through tides" [3]. Tides are predictable, which is also the greatest advantage that tidal energy has over other renewable sources like wind or solar power.

Horizontal axis tidal turbines (HATT) are also known as axial flow turbines; they have the rotational axis parallel to the tidal flow; thus, they operate in only one flow direction. The principle of operation of the HATT is similar to the horizontal axis wind turbine (HAWT); it has blades fitted to the hub, a generator to convert kinetic energy from the water to mechanical energy, shaft to produce power and gearbox [4]. There have been many advances in the development of the computational power and Computational Fluid Dynamics (CFD) models to simulate the complex flow around the turbine [5].

Some relevant studies on mesh independency techniques exist to improve the accuracy of the CFD simulations. The mesh independent solutions are entirely dependent on the mesh selected to resolve the fluid flow and the turbulence model that is chosen to illustrate the physics of the problem. The characteristics of a 10m diameter three-bladed HATT and the mesh was generated using ANSYS ICEM CFD (12C x 20C rectangular grid), which was very fine near the blade wall region to obtain precise results, but no y+ values were given in the source [6]. The authors found that by varying the thickness of the airfoil the hydrodynamic performance, as well as the strength of the blade, was good

 doi:10.20944/preprints201608.0008.v1

with the rotor producing a maximum efficiency of 47.6%. Another study, based on the mesh dependency of a tidal turbine blade, was performed by analysing the wake performance in non-uniform flow using the k-ε turbulence model and demonstrating using the two different profiles with the same coarse mesh settings. This produced small changes in the power coefficients of the two different rotors [7]. A numerical investigation and calibration of SST turbulence model were carried out to test the operational performance of a 'small scale horizontal axis wind turbine (SS-HAWT).' The grid sensitivity analysis exhibited the y+ of less than 5, including the blade tip to eliminate the discretisation error from the solution, and thus reduce the computational burden [8]. Four numerical techniques i.e. Grid Convergence Index (GCI), the fitting method, mesh refinement and General Richardson Extrapolation (GRE), were carried out to produce a mesh separated solution and for VAWT and to generate a power curve using CFD [9]. The CFD solution was produced using two turbulence models, SST and RNG k- ϵ. They achieved the mesh independent solution after converging the mesh solution and examining the iterative convergence error. Thrust and power coefficients of a 3D CFD tidal turbine model were validated with the experimental data especially at 15° and 20° of pitch angle and had a good agreement. The authors analysed the tidal turbine pressure, and near-wall effects were ANSYS's Shear Stress Transport (SST) also considering the mesh resolution and time step convergence [10].

The purpose of this paper is to investigate the mesh independency of a straight blade HATT, by employing two turbulence models namely the standard k-ε model and SST model, to keep the computational costs low. The grid convergence study was performed by developing three different meshes: with a coarse, medium, and fine grid for all six different meshes of the straight blade to predict the power, lift coefficients, and torque on normalised mesh cells to determine how the mesh quality affects CFD simulation results. The numerical results are compared and discussed in this present paper.

2. Methodology

2.1. *Non-dimensional forces acting on tidal turbine blades*

Water flow over an airfoil results in the production of forces distributed over the airfoil surfaces. As the fluid velocity increases over the airfoils, the 'convex surface' results in lower pressure on the 'suction' side when compared to the 'pressure side' of the airfoil. Hydrodynamic forces such as the drag, lift and torque (Figure 1) act on the airfoil when immersed in seawater due to its relative motion. These hydrodynamic forces arise due to pressure on the surface of the airfoil and the shear forces. Those forces are explained below:

- Lift force: This can be defined as the force that is perpendicular to the oncoming flow direction. The lift force is a result of the distribution of uneven pressure on the both upper and lower surfaces of the airfoil. Mathematically,

$$L = \frac{1}{2}\rho V^2 A C_L \quad (1)$$

- Drag force: This can be defined as the force that is parallel to the oncoming flow direction. The drag force is a result of both the distribution of uneven pressure on the both upper and lower surfaces of the airfoil and the viscous forces on the surface of the airfoil. Mathematically,

$$D = \frac{1}{2}\rho V^2 A C_D \quad (2)$$

- Pitching Moment (Torque) force: Torque force can be defined as the force which rotates around a perpendicular axis to the airfoil section.

Preprints (www.preprints.org) | NOT PEER-REVIEWED | Posted: 2 August 2016 doi:10.20944/preprints201608.0008.v1

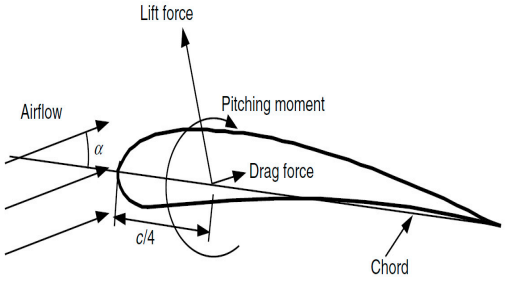

Figure 1. *Hydrodynamic forces acting on the airfoil*

Another important non-dimensional parameter which defines the airfoil flow characteristics is the Reynolds number, which can be defined as "the ratio of inertial forces to viscous forces and consequently quantifies the relative importance of these two types of forces for given flow conditions". Reynolds number is also used to differentiate the different flow patterns like Turbulent or Laminar flow. Thus, the Reynolds number (Re) can be defined as:

$$Re = \frac{\rho V L}{\mu} \tag{3}$$

where ϱ is the density of the sea water (kg/m^3), μ is the dynamic viscosity of sea water (kg/ms), V is the velocity of the seawater (m/s), and L is the characteristic length (m).

It is now possible to define the lift coefficient for a tidal turbine blade which can be expressed as:

$$C_L = \frac{L}{\frac{1}{2}\rho V^2 A} \tag{4}$$

The drag coefficient for a tidal turbine blade is defined as:

$$C_D = \frac{D}{\frac{1}{2}\rho V^2 A} \tag{5}$$

and the pitching moment (torque) coefficient for a tidal turbine blade can be defined as:

$$C_M = \frac{M}{\frac{1}{2}\rho V^2 A} \tag{6}$$

where ϱ is the density of the sea water (kg/m^3), V is the non-uniform velocity of sea water (m/s), A is the area of turbine blades (m^2), and M is the torque (N.m).

2.2. Turbine model

The straight blade was designed in ANSYS Design Modeller as shown in Figure 2. The airfoil considered for all the horizontal blades is a symmetrical NACA 0018. The spanwise distribution of the airfoils is done at every 10% of the blade. The distance between hub circle and the root airfoil is 20% of the total blade height.

Preprints (www.preprints.org) | NOT PEER-REVIEWED | Posted: 2 August 2016 doi:10.20944/preprints201608.0008.v1

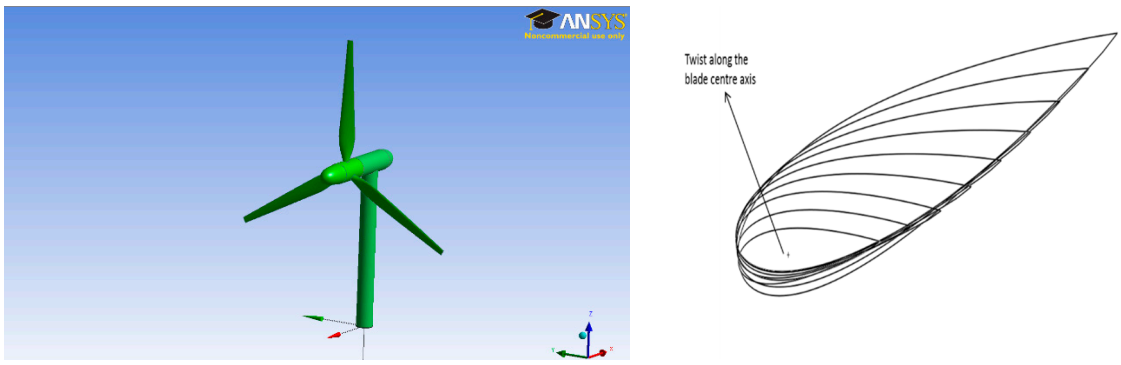

(**a**) (**b**)

Figure 2. **(a)** 3D model of the straight blade HATT; **(b)** Non-linear twist distribution

The blade hub is circular, and its diameter is 40% of the root airfoil chord length. The blade twist angle is higher at the root airfoil because it experiences less rotational forces and it gradually decreases across the entire span of the blade. The general blade parameters are given in Table 1.

Table 1. Straight blade parameters

Number of blades	**3**
Radius	7.4 m
Airfoil	NACA 0018
Root airfoil chord length	1 m
Tip airfoil chord length	360 mm
Root airfoil twist	16°
Tip airfoil twist	4°

2.3. Standard k-epsilon (k-ε) turbulence model

The k-epsilon (k-ε) turbulence model is the most widely used in CFD to analyse and simulate the turbulent flow conditions. It is a two-equation turbulence model as it describes the result for conservation equations using two transport equations k and epsilon. This model is an improvement to the mixing length model as it has good stability for high Reynolds number turbulent flow [11]. The first transport model k-equation arbitrates the energy from the turbulent kinetic energy equation and is described as turbulent kinetic energy (k). The second transport model is the dissipation of turbulence (ε), which describes the rate at which turbulent kinetic energy dissipates. The experimental form for the standard k-ε model can be described as [12]:

$$\frac{\partial(\rho k)}{\partial t} + \nabla.(\rho k\bar{u}) = \nabla\left[\frac{\mu_t}{\sigma_k}\nabla.k\right] + P - \rho\epsilon \tag{7}$$

$$\frac{\partial(\rho \epsilon)}{\partial t} + \nabla.(\rho \epsilon\bar{u}) = \nabla\left[\frac{\mu_t}{\sigma_\epsilon}\nabla.\epsilon\right] + C_{1\epsilon}\frac{\epsilon}{k}P - C_{2\epsilon}\,\rho\frac{\varepsilon^2}{k} \tag{8}$$

where u_i is the velocity component in parallel direction, E_{ij} is the rate of deformation, $\mu_t = C_\mu \rho \frac{k^2}{\epsilon}$ is the eddy viscosity, and $P = 2\mu_t S_{ij}.S_{ij}$

2.3. Shear Stress Transport (SST) turbulence model

The SST model was developed by Menter [13]; it assimilates the inner and outer region of the boundary layer in between the eddy viscosity and full turbulent viscosity formation. The SST model draws up the best effects of k-ε (accurate precision of results in the far field region) and k- ω (good accuracy in providing results in the near wall region), it being used as low Reynolds number model

Preprints (www.preprints.org) | NOT PEER-REVIEWED | Posted: 2 August 2016 doi:10.20944/preprints201608.0008.v1

without any blending functions changes the cross term function) also prevents being too sensitive to 'inlet free stream turbulence'.

$$\frac{\partial(\rho\omega)}{\partial t} + \nabla.(\rho\omega\bar{u}) = \nabla\left[\mu + \frac{\mu_t}{\sigma_{\omega,1}}\nabla.\omega\right] + \gamma_2\left(2\rho S_{ij}.S_{ij} - \frac{2}{3}\rho\omega\frac{\partial\bar{u}_i}{\partial x_j}\delta_{ij}\right) - \beta_2\rho\omega^2 + 2\frac{\rho}{\sigma_{\omega,2}\omega}\frac{\partial k}{\partial x_k}\frac{\partial\omega}{\partial x_k} \quad (9)$$

3. Mesh Independency study

To establish the accuracy of the CFD solution, and to keep the computational costs low, the straight blade was analysed using: the standard k-ε model, and SST model, at uniform V_{in} = 2.5m/s, and λ = 5. The grid convergence study was performed by developing three different meshes: with a coarse, medium, and fine grid for all six different meshes of the Straight Blade to predict the power, lift coefficients, and torque on normalised mesh cells to determine how the mesh quality affects CFD simulation results.

The number of nodes and the simulation time for the three cases simulated using the SST model are highlighted in Table 2, and the three cases simulated using the standard k-ε model are given in Table 3. Table 2, and 3 summarise the key characteristics of the meshes, and it is very clear that CFD simulation time is highly dependent on the number of mesh nodes considered. The six meshes generated have near wall resolution i.e. y+ < 10 by using the standard wall function approach to avoid unsatisfactory results when using the standard k – ε model.

Table 2. Mesh size, CFD simulation time, and estimated C_P for SST model at λ = 5

Mesh Resolution	Coarse Mesh (M1)	Medium mesh (M2)	Fine mesh (M3)
Number of nodes	79859	151740	230439
CFD simulation time	4hrs 10mins	6hrs 16mins	9hrs 53mins
Estimated C_P	0.3816	0.4169	0.4218

Table 3. Mesh size, CFD simulation time, and estimated C_P for k-ε model at λ = 5

Mesh Resolution	Coarse mesh (M4)	Medium mesh (M5)	Fine mesh (M6)
Number of nodes	44064	92767	139506
CFD simulation time	1hr 36mins	4hrs 41mins	5hrs 38mins
Estimated C_P	0.2271	0.2586	0.2693

In the case of the investigated meshes of the straight blade, the turbine domain has an increased mesh resolution due to the blades being exposed to the complex flow separation. The mesh is refined in the grids from M1 to M6 where M1, M2, M3 represent coarse, medium, and fine mesh generated for the SST turbulence model; and M4, M5, M6 represent coarse, medium, and fine mesh generated for the standard k-ε turbulence model. The estimated power coefficient increased from 0.2271 to 0.4218 as shown in Figure 3.

Preprints (www.preprints.org) | NOT PEER-REVIEWED | Posted: 2 August 2016 doi:10.20944/preprints201608.0008.v1

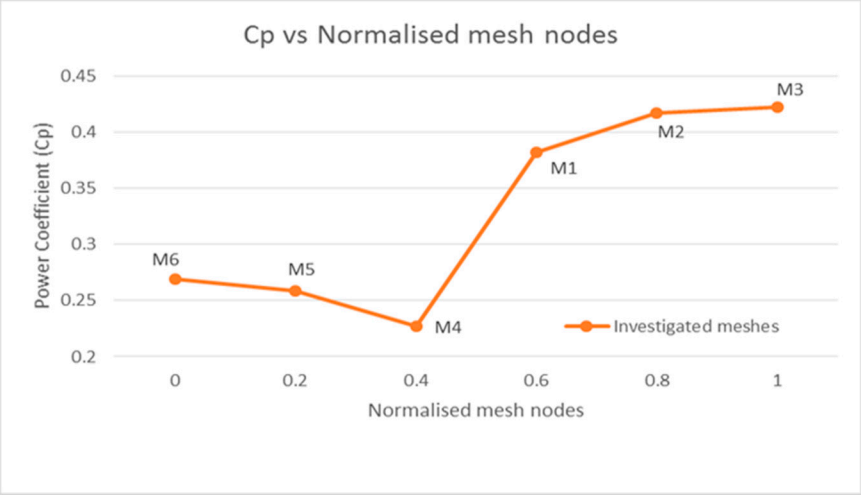

Figure 3. The power coefficients of all the investigated meshes in mesh independency study

It is important to note that the mesh resolution plays a pivotal role in the final CFD results. The mesh nodes need to be small to resolve the boundary layer on the blade surfaces. The highest CP obtained from the mesh independent study is 0.4218 for M3 from the SST model. M2 and M3 account for nearly 1% difference in the estimated power coefficients, but the final CFD simulation time required for convergence of the two meshes has a significant difference when the conventional mesh independency method is employed. The power coefficients obtained from the standard k-ε model are almost 15% to 20% lower than the SST model power coefficients, which is due to the poor performance of the k-ε model in near-wall regions and in adverse pressure gradients i.e. the fluid flow near the turbine blade surfaces; which causes the k-ε model to underestimate the power coefficient.

It is clear from the final CFD simulation results that the simulation time is highly dependent on the number of mesh nodes, and the turbulence model selected. As shown in Figure 3 when using k-ε model for all the meshes (M4, M5, and M6) employed the CFD solution under predicts power coefficient when compared with the SST model. M1 leads to the reasonable prediction of the power coefficient on the straight blade, whereas the power coefficient of M3 is slightly better than M2. Due to the slight difference medium mesh (M2) is best regarding computational costs and is further employed for the numerical analysis carried out in the following section of the turbulence model comparison study.

3.1. Turbulence model comparison study

To understand the sensitivity of the CFD solution a consecutive study was carried out with these turbulence models at medium sized meshes. From the mesh dependency test conducted it has been found that the SST model performs superiorly in adverse pressure gradient situations than the standard k-ε model; because SST model is a unification of k-ε model and k-ω model for free stream and inner boundary layer problems respectively. Figure 4 shows the torque coefficient related to each of the two turbulence models analysed for the medium mesh. As shown in Figure 4 the SST model medium mesh has higher CM than the standard k-ε model in all the nine different TSR's. It can also be seen that the torque coefficient of SST medium mesh model increased by more than 25% when compared to the standard k-ε model medium mesh.

Preprints (www.preprints.org) | NOT PEER-REVIEWED | Posted: 2 August 2016 doi:10.20944/preprints201608.0008.v1

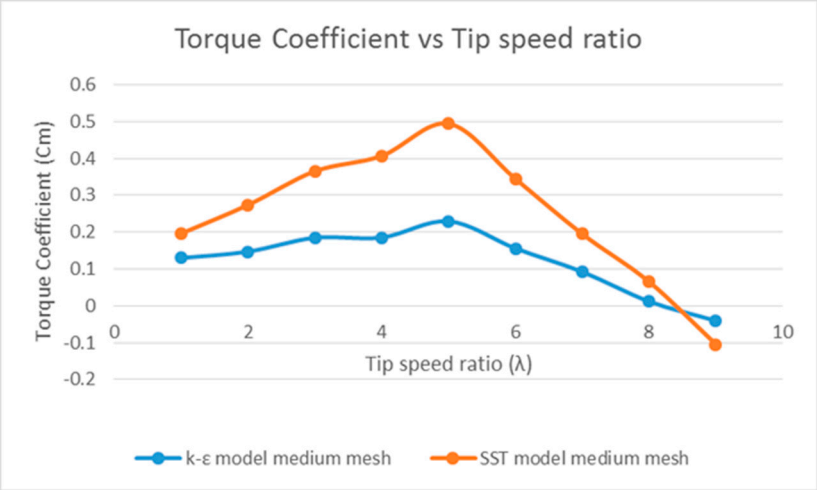

Figure 4. Torque coefficient versus Tip speed ratio for k-ε and SST model medium meshes

The highest CM is achieved at $\lambda = 5$ for both the cases, CM increases with the increasing TSR and acts as a function of TSR. It can also be noted that the non-linearity in the torque coefficient occurs after TSR of 5, and the k-ε model fails to capture this, due to the boundary layer and turbulence quantities to the blade wall.

Figure 5 shows that the power coefficient increases steadily until TSR ≈ 5, at which it shows the peak CP ≈ 0.4169 for the SST model medium mesh; after which it shows a drastic reduction with the increasing $\lambda > 6$. The curve for medium mesh the k-ε model shows that it predicts a lower power coefficient to a satisfying level of accuracy, and also under predicts the values with increasing λ. However, the numerical CP prediction by medium mesh the SST model observed values are approximately 20% higher than medium mesh the k-ε model simulation, the range $5 \leq \lambda \leq 6$ was also validated [10, 14]; and considered to be optimum range for HATT. The standard k-ε model is incapable of capturing the account of rotational forces and their effects on the turbine blades, and due to the near wall physics implementation. Thus the CP prediction by SST model is more acceptable when compared to the power coefficient predictions by the standard k-ε model.

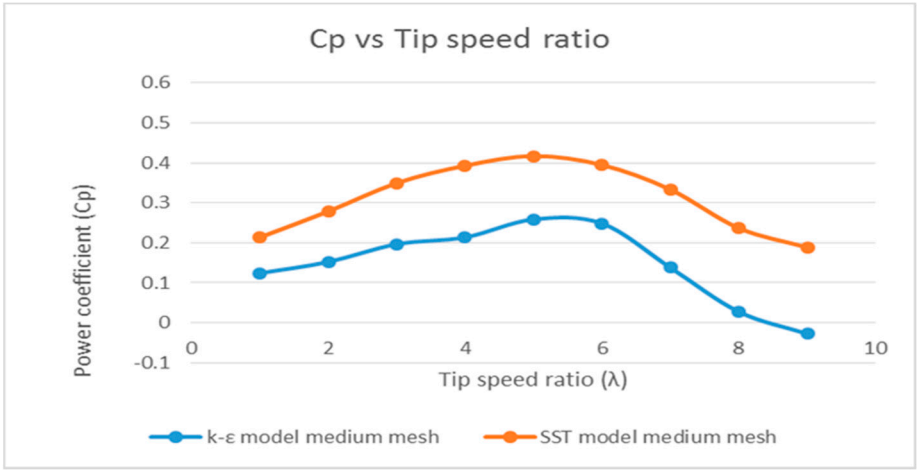

Figure 5. Power coefficient versus tip speed ratio for k-ε and SST model medium meshes

As a result of the mesh independency test conducted it can be concluded that the overall power coefficient shown by the SST turbulence model is more reasonable than the standard k-ε model, for all the cases considered. Therefore to avoid any misleading CFD results the standard k-ε model is not employed in any further CFD tests conducted in this research. The power coefficient of a HATT is

Preprints (www.preprints.org) | NOT PEER-REVIEWED | Posted: 2 August 2016 doi:10.20944/preprints201608.0008.v1

highly sensitive to the turbulence model chosen for the CFD analysis; however the mesh independent CFD solution for SST medium mesh satisfactorily achieves the mesh independency over the SST fine mesh solution which requires a massive computational overhead. Hence, the medium mesh is used to conduct the steady state analysis in following sections.

4. Steady state analysis using SST model

4.1. Meshing and boundary conditions

The three-dimensional modelling and steady state simulations presented in this section are conducted using ANSYS CFX, using the Shear Stress Transport model to solve the Reynolds Averaged Navier-Stokes (RANS) equations for the unstructured mesh approach is used to predict the highest efficiency generating blade. The computational mesh is finer near the turbine disc area and coarser on the seawater domain modelled in the unstructured pattern to improve the accuracy of the CFD simulation.

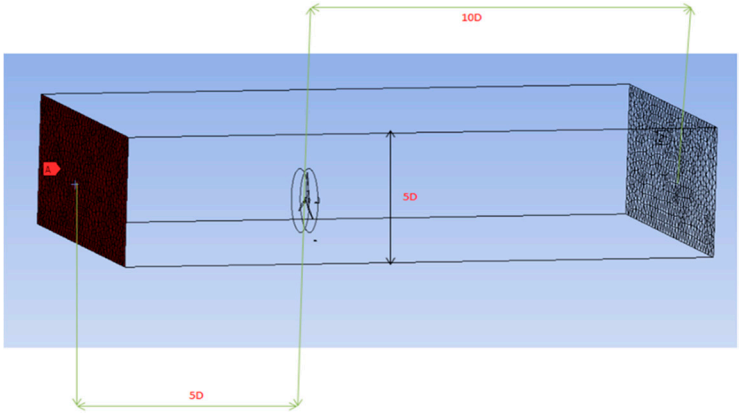

Figure 6. Inlet, outlet, and height extension from the turbine blades

Figure 6 shows the rectangular computational grid which was used to model the seawater domain and the turbine disc domain, for the straight blade. The seawater domain extends five times the turbine diameter at the inlet and ten times of the turbine diameter at the outlet, and the height of the rectangular grid is five times of the turbine diameter. The turbine domain was designed as 'rotating domain in CFX, and then a full 360° mesh surrounding the tidal turbine blades. An unstructured tetrahedral mesh was constructed around this domain as the flow would be highly non-linear, and the rotational effects are to be considered. Figure 7 shows the blade meshing including the hub and tips of the blade.

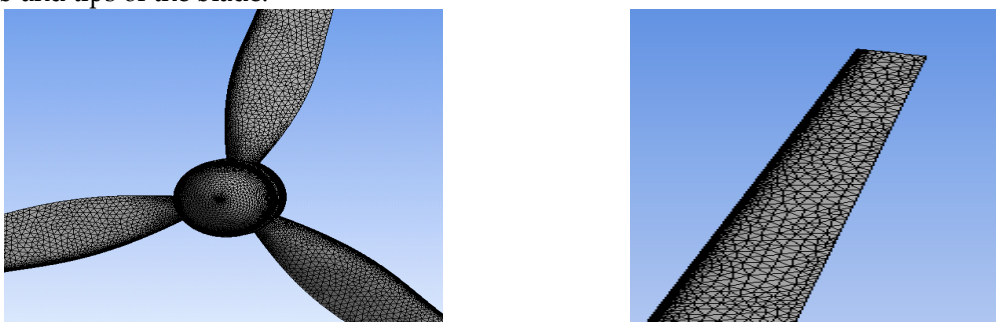

(**a**) (**b**)

Figure 7. (a) Meshed SB with blades and hub, (b) SB meshed tip

In the meshing aspect, the tetra-prism mesh consisted of 151740 nodes, including the turbine disc rotating domain. The three-dimensional modelling and steady state CFD simulations presented in this paper are conducted using ANSYS CFX, the fluid was defined as seawater and was simulated

Preprints (www.preprints.org) | NOT PEER-REVIEWED | Posted: 2 August 2016 doi:10.20944/preprints201608.0008.v1

at constant inlet velocity of 2.5m/s, using high turbulence intensity of 10%. The outlet pressure was defined as 0bar, the blade was defined as a 'Rotating Wall', with no slip wall condition, for mass and momentum option. The bottom and side walls were defined as free slip walls to incorporate the accuracy when solving the continuity equation. The front and back walls were defined as inlet and outlet walls respectively. The SST turbulence model was chosen to predict the accurate hydrodynamic flow and pressure gradients on the airfoil, and also because of its good prediction of the boundary layer separation. The calculations were performed with an Intel (R) Xeon (R) (3.30GHz*2). The convergence condition was determined in a margin error less than 10^{-5}, and simulating each case study required at least three h.

5. Results and Discussion

As the seawater flow velocity progressed over the blade pressure side, the pressure increased primarily on the tip of the blade as it was affected due to the rotational velocity being the highest on the tip. At the same time flow velocity at the same time decreased; which further resulted in arduous movements on the blade suction surface except on the trailing edge of the blades. Figure 8 shows the pressure distribution on the Straight blade (blades rotate anti-clockwise).

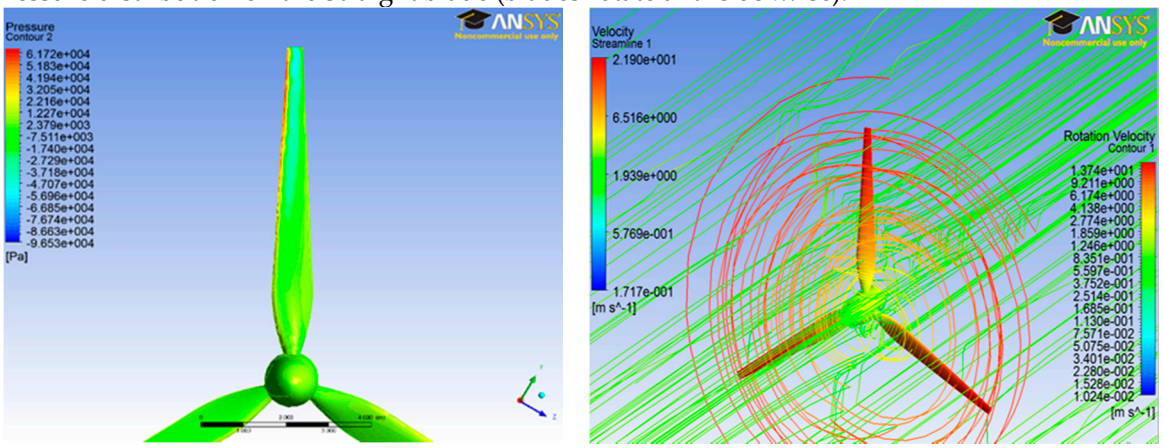

(**a**) (**b**)

Figure 8. (a) Meshed SB with blades and hub, (b) SB meshed

Figure 8 also shows blade rotational velocity and streamlines on the case study performed, and the fluid velocity expands as it passes through the turbine and causing it to produce maximum efficiency. It can also be seen that the positive blade tip vortex are seen on the pressure side of the blade, this is because of the high turbulence intensities generated from the trailing edge of the airfoil and thus creating downstream interaction of the Reynolds shear stress and turbulent boundary layer formation. The NACA 0018 airfoil, a high lift generating airfoil, generates lift from the pressure difference created by the fluid and blade interaction. The varying lift coefficient distribution can also be demonstrated by plotting the mid-height coefficient of lift distributions on the straight blade, and can be demonstrated in Figure 9. The highest lift coefficient at 0.5 blade span location with a peak value of 0.182, and leading edge contributes to the pressure distribution increase on the pressure side, but at the same time the trailing edge causes the negative pressure distribution increase on the suction side; thus contributing to lift force decrement and torque force reduction as well. The straight blade produces 366 kW of power, and power coefficient of 0.4028%.

Preprints (www.preprints.org) | NOT PEER-REVIEWED | Posted: 2 August 2016 doi:10.20944/preprints201608.0008.v1

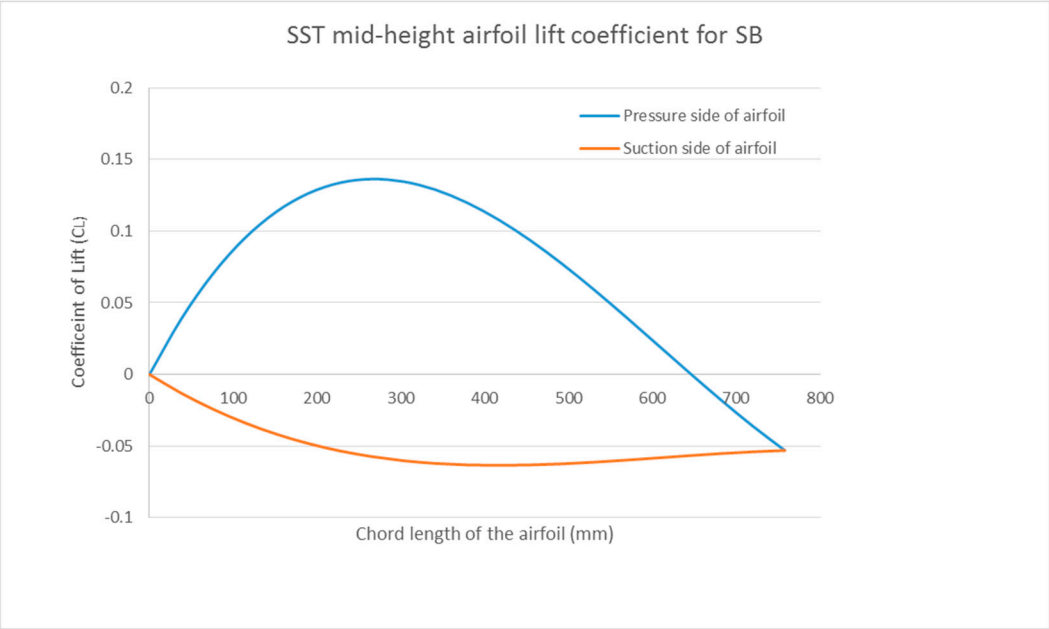

Figure 9. SST mid-height lift coefficient distribution for the straight blade

6. Conclusions

This paper presented a mesh independency study of a straight blade to determine the mesh sensitivity and its effects on the CFD simulation results. The grid convergence study was simulated using two turbulence models: the standard k-ε model, and SST turbulence model at coarse, medium, and fine mesh resolution thus simulating six different mesh sizes. This paper has shown that obtaining mesh independent solutions is a fundamental need for all the tidal turbine blade designers due to the sensitivity of the lift coefficient of the tidal turbine.

The standard k-ε model under predicts the power coefficients and the simulation time is highly dependent on the mesh and turbulence model chose for CFD analysis. The highest CP obtained from the mesh independent study conducted is 0.4218 for M3 from SST model and the lowest CP 0.2693 for M6 using k-ε model. M2 and M3 account for nearly 1% difference in the estimated power coefficients, but the final CFD simulation time required for convergence of the two meshes is substantially different when conventional mesh independency method is employed.

The power coefficients obtained from the standard k-ε model are almost 15% to 20% lower than the SST model power coefficients, due to the poor performance of the k-ε model in near-wall regions and in the adverse pressure gradient which causes the k-ε model to underestimate the power coefficient. The SST medium mesh offers the best level of accuracy regarding computational costs.

Acknowledgements: The authors are grateful for the financial support from the Birmingham City University, Birmingham, UK. This work is the outcome of the first author's PhD thesis. Professor Craig Chapman, and Professor Hanifa Shah have supervised his PhD work and have provided excellent technical, and philosophical support respectively. The first author sincerely thanks, Professor Peter Larkham for comments on the draft version of this report.

Conflicts of Interest: The authors declare no conflict of interest.

References

1. Shi, W.; Wang, D.; Altar, M.; Guo, B.; Seo, K. Optimal design of a thin-wall diffuser for performance improvement of a tidal energy system for an AUV. *Ocean Engineering* **2015**, *Volume 108*, 1 – 9, DOI: https://doi.org/10.1016/j.oceaneng.2015.07.064
2. Tedds, S.; Owen, I.; Poole, R. Near-wake characteristics of a model horizontal axis tidal stream turbine. *Renewable Energy* **2014**, *Volume 63*, 222 – 235, DOI: http://dx.doi.org/10.1016/j.renene.2013.09.011
3. Blunden, L.; Bahaj, A. Initial evaluation of tidal stream energy resources at Portland Bill, UK. *Renewable Energy* **2006**, *Volume 31*, 121-132, DOI: http://dx.doi.org/10.1016/j.renene.2005.08.016

4. Bai, G; Li, W.; Chang, H.; Li, G. The effect of tidal current directions on the optimal design and hydrodynamic performance of a three-turbine system. *Renewable Energy* **2016**, *Volume 94*, 48 – 54, DOI: https://doi.org/10.1016/j.renene.2016.03.009
5. Malki, R.; Masters, I.; Williams, A.; Croft, T. Planning tidal stream turbine array layouts using a coupled blade element momentum – computational fluid dynamics model. *Renewable Energy* **2014**, *Volume 63*, 46-54, DOI: http://dx.doi.org/10.1016/j.renene.2013.08.039
6. Goundar, J; Ahmed, M. Design of a horizontal axis tidal turbine. *Applied Energy* **2013**, *Volume 111*, 161 – 174, DOI: http://dx.doi.org/10.1016/j.apenergy.2013.04.064
7. Masters, I.; Malki, R.; Williams, A.; Croft, T. The influence of flow acceleration on tidal stream turbine wake dynamics: A numerical study using a coupled BEM–CFD model. *Applied Mathematical Modelling* **2013**, *Volume 37*, 7905-7918, DOI: http://dx.doi.org/10.1016/j.apm.2013.06.004
8. Costa Rocha, P.; Barbosa Rocha, H.; Carneiro, F.; Viera da Silva, M.; Bueno, A. k-ω SST (shear stress transport) turbulence model calibration: A case study on a small scale horizontal axis wind turbine. *Energy* **2014**, *Volume 64*, 412-418, DOI: https://doi.org/10.1016/j.energy.2013.11.050
9. Almohammadi, K.; Ingham, D.; Ma, L.; Pourkashan M. Computational fluid dynamics (CFD) mesh independency techniques for a straight blade vertical axis wind turbine. *Energy* **2013**, *Volume 58*, 483 – 493, DOI: http://dx.doi.org/10.1016/j.energy.2013.06.012
10. McSherry, R.; Grimwade, J.; Jones, I.; Mathias, S.; Wells, A.; Mateus, A. 3D CFD modelling of tidal turbine performance with validation against laboratory experiments. The European Wave and Tidal Energy Conference, Southampton, UK, 2011.
11. Launder, B.; Reece, G.; Rodi, W. Progress in the development of a Reynolds-stress turbulence closure. *Journal of Fluid Mechanics* **1975**, *Volume 68*, 537-566, DOI: http://dx.doi.org/10.1017/S0022112075001814
12. Wilcox, D. *Turbulence modelling for CFD*, 2nd ed.; DCW Industries, Inc. La Canada, California, United States, 1994; pp. 83-95
13. Menter, R. Zonal Two-Equation Kappa-Omega Turbulence Models for Aerodynamic Flows. AIAA Fluid Dynamics Conference, Orlando, FL; United States, 6-9 Jul. 1993.
14. Bahaj, A.; Molland, A.; Chaplin, J.; Batten, W. Power and thrust measurements of marine current turbines under various hydrodynamic flow conditions in a cavitation tunnel and a towing tank. *Renewable Energy* **2007**, *Volume 32*, 407 – 426, DOI: http://dx.doi.org/10.1016/j.renene.2006.01.012